RSC Advances

PAPER

View Article Online
View Journal | View Issue

Cite this: *RSC Adv.*, 2024, **14**, 3675

The use of banana peel as a low-cost adsorption material for removing hexavalent chromium from tannery wastewater: optimization, kinetic and isotherm study, and regeneration aspects†

Bereket Ameha,[a] Talbachew Tadesse Nadew,[b]* Tsegaye Sissay Tedla,[c] Belay Getye,[d] Destaw Agumass Mengie[a] and Shiferaw Ayalneh[c]

When the concentration of hexavalent chromium (Cr(VI)) in the environment is greater than a certain limit, it becomes a global concern. Thus, the aim of this study was to use banana peel as an adsorbent to remove heavy metals, specifically Cr(VI) ions from wastewater. Banana peel (BP) was activated in a furnace for 2 h (h) at 450 °C and 50% humidity. Subsequently, the activated BP was characterized by proximate analysis, elemental analysis, scanning-electron microscopy (SEM), X-ray diffraction (XRD), Fourier transform infrared spectroscopy (FTIR), Brunauer Emmett Teller (BET) analysis, and thermogravimetric analysis (TGA). According to the characterization results, the activated BP possessed a porous surface and high surface area of 200 $m^2\ g^{-1}$, which are important adsorption parameters. Additionally, the removal efficiency for Cr(VI) was evaluated in terms of pH, contact time, initial concentration, and adsorbent dose. Consequently, the optimal operating conditions for removing 94% of Cr(VI) were found to be an adsorption time of 92 min, adsorbent dose of 1.5 g L^{-1}, pH of 3, and initial Cr(VI) concentration of 38 mg L^{-1}. In addition, the adsorption kinetics and isotherms were examined. The pseudo-first-order model with an R^2 of 0.996 and the Langmuir isotherm with an R^2 of 0.997 were found to be the most effective mathematical representations of the rate and nature of Cr(VI) adsorption on the surface of the activated BP, respectively. Furthermore, it was discovered that the activated BP could be reused six times before its removal efficiency was reduced to less than 70%.

Received 2nd November 2023
Accepted 8th January 2024

DOI: 10.1039/d3ra07476e

rsc.li/rsc-advances

1. Introduction

Hazardous compounds have spread in the aquatic environment at an unprecedented rate as a result of the global Industrial Revolution.[1] Specifically, various manufacturing sites are responsible for polluting fresh water and the ecosystem with their wastewater containing different heavy metals,[2] including the leather tanning, electronics, metal finishing, electroplating industries, if they discharge their effluents without treatment.[3]

Heavy metals are also present in water bodies as a result of home and agricultural contaminants. Besides, various inorganic and organic contaminants are present in the effluents of industries. Heavy metals, for example, alter the chemical composition of diverse water sources, while also posing a major health risk due to their toxicity.[4,5] Large amounts of heavy metals such as lead (Pb), zinc (Zn), copper (Cu), arsenic (As), cadmium (Cd), chromium (Cr), nickel (Ni), and mercury (Hg) are among the heavy metals from various industries that are the most concerning.[6,7] Thus, contamination with these heavy metals has become a significant issue globally. Although humans require trace amounts of heavy metals such as copper and zinc, high levels of these metals can be dangerous.[8]

Naturally, heavy metals can be found immobilized in sediments and as ores. However, due to anthropogenic activity, there is an increase in heavy metal deposition in the aquatic and terrestrial environments as a result of these metals becoming mobilized and released as well as natural biogeochemical cycles being upset.[9] Hexavalent chromium is one of the many heavy metals that contaminates water from the paint, alloying, animal hide tanning, textile, dye, pigment, ceramic glaze, refractory brick, and pressure-treated wood industries.[10] Thus, because of the extensive anthropogenic use of chromium, its environmental pollution is increasing. This pollutant causes various diseases, including cancer, nephritis, gastrointestinal

[a]Department of Chemical Engineering, Faculty of Chemical and Food Engineering, Bahir Dar Institute of Technology, Bahir Dar University, Bahir Dar, Ethiopia
[b]Department of Chemical and Food Engineering, Kombolcha Institute of Technology, Wollo University, Dessie, Ethiopia. E-mail: talewtadesse4897@gmail.com
[c]Department of Chemical Engineering, College of Biological and Chemical Engineering, Addis Ababa Science and Technology University, Addis Ababa, Ethiopia
[d]Department of Industrial Chemistry, College of Applied Science, Addis Ababa Science and Technology University, Addis Ababa, Ethiopia

† Electronic supplementary information (ESI) available. See DOI: https://doi.org/10.1039/d3ra07476e

ulceration, and perforation in a partition of the nose, affect the central nervous system and cause respiratory issues and lung tumors when inhaled.[8,11] Thus, chromium-containing effluents requires treatment before their discharge in the environment due to their carcinogenic and mutagenic properties. In this case, adsorption *via* activated carbon (AC) is a popular and effective method for treating wastewater that contains metals such as chromium.[12]

To date, a variety of methods have been developed for the removal of chromium from wastewater, including coagulation, flocculation, membrane processes, ion exchange, and chemical precipitation. However, these methods are limited, given that they often involve high capital and operational costs. Also, most of these methods are not suitable for application on a small scale because of their high operational costs and use of excess chemicals and disadvantages such as incomplete metal removal and production of sludge.[13]

Currently, most industries release wastewater containing heavy metals, which can be absorbed in living tissues, causing various disorders.[14] There are numerous sources of waste biomass in nature with reported adsorption properties, including rice husk, sawdust, tea and coffee waste, orange peel, peanut shells, dry tree leaves, and bark.[15] Among the different categories of adsorbents, BP seems to be a suitable adsorbent because of its low cost and environmentally friendly nature. Because of the excess BP waste worldwide, it is considered to be a low-cost adsorbent with promising application for the remediation of a variety of contaminants. BP has diverse functional groups, which enable the high sorption of various cationic and anionic substances on its surface active sites.[16] However, although the use of BP for adsorption was previously studied, the potential of activated BP in treating actual tannery wastewater has not been reported to date. To the best of our knowledge, there are no studies in the literature on the removal of chromium from actual industrial wastewater using BP; however, the majority of current research has demonstrated the application of banana peel for the removal of specific heavy metals and dye from a standard solution.

An inexpensive and eco-friendly material for the possible removal of chromium from wastewater is activated BP. This study aimed to synthesize activated BP from BP and examine its potential application as an adsorbent for the removal of hexavalent chromium from tannery wastewater. The primary motivations for removing heavy metals from contaminated wastewater are to protect the environment and prevent human health concerns caused by direct emissions from various industrial processes. Furthermore, this study has the potential to reduce the threat of industrial wastewater polluted with Cr(VI) to human help and equip the community with a simple and cheap technique for treating water.

2. Materials and methods

2.1 Raw materials and chemicals

The raw BP sample was collected from the surrounding garbage using a polyethylene bag. The chromium-containing wastewater required for the study was obtained from the Batu Leather Industry, which is located around Akaki Kality Sub-city, Addis Ababa, Ethiopia. The chemicals used were sodium hydroxide (NaOH) (98%, Sigma-Aldrich, USA), hydrochloric acid (HCl) (37%, Sigma-Aldrich, USA), phosphoric acid (H_3PO_4), potassium dichromate ($K_2Cr_2O_7$) (99.9%, Sigma-Aldrich, USA), and 1,5-diphenylcarbazide ($C_{13}H_{14}N_4O$) (98.0%, Sigma-Aldrich, USA). These chemicals were purchased from commercial sources in Addis Ababa, Ethiopia, and used as received without further purification.

2.2 Methods

2.2.1 Material preparation. BP was collected, washed repeatedly with distilled water to eradicate impurities, and then dried in an oven at 60 °C for 24 h. The dry sample was kept at room temperature in a plastic bowl for further experiments. The standard Cr(VI) solution with a concentration of 1000 ppm was prepared by mixing 2.835 g potassium dichromate in 1 L distilled water. The required initial Cr(VI) concentration was obtained by adding pure water to the standard solution, and the adsorption process was tested in an incubation shaker.

2.2.2 Preparation of adsorbent from waste banana peel. To scrutinize the favorable activation parameters and the corresponding parameters, a preliminary study was conducted. Specifically, the activation temperature, activation time, and acid (phosphoric acid) concentration were the parameters considered for the activation process, as presented in Table 1. Firstly, the waste BP was ground and sieved. Then, 50 g of prepared BP was transferred to conical flasks containing 10%, 30%, 50%, 70%, and 90% phosphoric acid in a wt./wt. ratio at a fixed activation temperature of 450 °C. Then, the flasks were covered with aluminum foil and leftover for 2 h. The treated samples were washed carefully with distilled water, moved to labeled clean dry crucibles, dried at 105 °C in an oven for 24 h, and kept in a desiccator to remove moisture prior to carbonization. Then, the samples in the crucibles placed in a furnace at 350 °C, 400 °C, 450 °C, 500 °C, and 550 °C at a fixed time of 2 h and an acid concentration of 50% to study the effect of the activation temperature. Similarly, the activation time was varied to 1, 1.5, 2, 2.5, and 3 h at a fixed activation temperature of 450 °C and acid concentration of 50%.

After carefully washing and rinsing each sample by vacuum filtration with hot distilled water to remove all the excess acid, the pH of the filtrate was roughly 7.0. Then, it was dried for 24 h at 105 °C in an oven and stored in a desiccator for additional analysis.[17] To study the effect of the activation parameters on BP, 40 mg L^{-1} hexavalent chromium solution was absorbed on the surface of 1.5 g L^{-1} BP. The contact time and pH were kept at 90 min and 3, respectively. The removal efficacy was quantified using a UV-spectrophotometer and calibration curve.

2.3 Characterization

2.3.1 Proximate analysis. The proximate results (moisture content, volatile matter, fixed carbon, and ash content) of the raw and activated BP were determined using the American Society for Testing and Materials (ASTM D2866-2869) standard techniques.[18]

Table 1 Parameter level for the BP activation process

Varying parameter	Parameter level	Fixed parameter
Activation time (h)	1–3	450 °C and 50% of acid concentration
Activation temperature (°C)	350–550	2 h time and 50% of acid concentration
Acid concentration (%)	10–90	2 h time and 450 °C temperature

2.3.2 Elemental analysis. Elemental analysis is crucial in determining the potential application of BP for the adsorption of hexavalent chromium and it environmental impact and suitability. The elemental analysis of raw BP and activated BP was investigated using a CHNS/O analyzer (EMA 502, VELP China). The elemental composition carbon (C), hydrogen (H), nitrogen (N), and sulfur (S) of both the raw and activated BPs were examined using 5 mg of powder samples in clean tin cups with the ASTM testing method (D5373). The samples were completely dried sample with a moisture content of less than one percent. The elemental analyzer was calibrated, and the combustion furnace set at a temperature of 1060 °C. The results were automatically calculated by the EMASoft™ software receiving real-time data in terms of elemental weight percentage from the atomic ratio for each element. For the determination of the percentage of oxygen (O), the sum of C, H, N, and S was subtracted from 100%.

2.3.3 Brunauer Emmett Teller (BET). A BET (Horiba 96 000 series) surface area analyzer was used to determine the surface area of the adsorbent. The procedure and operation involved using 0.8 g of sample, and then heating it at a temperature of 110 °C for 2 h to remove the moisture content. Then, the sample was weighed again after cooling, and its weight recorded. The prepared sample was transferred to the surface area test part of the BET. The pore size distribution was determined using the Barrett–Joyner–Halenda method. The surface area of the sample was calculated using the nitrogen adsorbed–desorbed multipoint data and the surface area of a single nitrogen molecule.[19]

2.3.4 Fourier transform infrared spectroscopy (FT-IR). The functional groups on the surface of the adsorbent or AC BP (before and after adsorption, respectively) were studied using FT-IR (Fourier Transform Infrared, PerkinElmer, USA) analysis. Briefly, 2 g sample was mixed with 0.3 g of anhydrous KBr, and the mixture was pressed using a hydraulic press and put in the FTIR spectrometer. Subsequently, the spectrum was recorded in the wavenumber range of 400–4000 cm^{-1}.[20]

2.3.5 Scanning electron microscopy (SEM). The morphological structure of the raw and activated BP before and after adsorption was investigated using SEM (FEI, INSPCT-F50, Germany). The procedure and operating conditions were set according to the method used by J. F. Nohl *et al.*[21]

2.3.6 X-ray diffraction (XRD). The crystallographic structure formed in the activated BP was analyzed using an X-ray diffractometer (XRD-7000S, Cu-Kα radiation) operating at a voltage of 40 kV and current of 30 mA in a continuous scanning path. The data (2θ *versus* intensity) was recorded in the 2θ range of 10–80° and plotted using Origin (OriginPro 2018). The average crystal size of the activated BP was calculated using the Scherrer equation.[22]

2.3.7 Thermogravimetric analysis (TGA). TGA (DTG-60H, Shimadzu, Japan) was used to analyze the effect of temperature on the raw and activated BP, where 10 g of sample was heated from ambient temperature to 800 °C and its decomposition was recorded by the gravimetric analyzer.[23]

2.3.8 Point of zero charge (pzc) determination. The pzc is the point on the adsorbent surface where the net charge is zero.[24] The pH of the solution and its point of zero charge (pHpzc) determine the surface charge of the adsorbent. When the pH is greater than pH_{pzc}, the adsorbent surface will be negatively charged, whereas it is positively charged if the pH is less than pH_{pzc}. Briefly, 1.5 g of adsorbent was added to 45 mL of 0.1 N KNO_3 solution with a pH value in the range of 2 to 14. Drops of 0.1 N HCl and NaOH solutions were added to the initial pH solution to adjust it. Each flask was closed and thoroughly shaken for 48 h at room temperature. Finally, the pH level was determined and recorded. The difference between the initial pH and the pH after 48 h was used to calculate the net charge (pH) on the activated BP surface. The experiment data were plotted with the pH values along the *x*-axis and ΔpH along the *y*-axis. The intersection point was used as the reference to calculate pHpzc.[25]

2.4 Batch adsorption experiments on activated BP

To investigate the chromium adsorption capacity of the activated BP under different operating conditions, one variable at a time (OVAT) and response surface methodology (RSM) experiments were performed. The results of OVAT were used as the feed for the interaction effects. The parameter interaction effects on the adsorption processes were investigated using RSM and CCD (central composite design).[26]

After reviewing various articles in the literature, four parameters (contact time, adsorbent dose, pH, and initial chromium concentration) were considered to have a high influence on adsorption processes, and thus chosen to for the experiment. To analyze the effect of each variable, the chemicals used in UV-spectrophotometry were prepared following ASTM standard procedures.

2.4.1 Preparation of diphenyl carbazide and Cr(VI) stock solutions. Briefly, 0.25 g diphenyl carbazide was weighed, dissolved in 25 mL acetone, and then mixed thoroughly. Then, using deionized water, the solution was diluted to a final volume of 50 mL. This reagent was stored in an amber glass bottle and kept in a refrigerator.[27] Potassium dichromate ($K_2Cr_2O_7$) was used as the source of hexavalent chromium.

Briefly, 2.835 g of 99% $K_2Cr_2O_7$ crystals was dissolved accurately in 1 L of double-distilled water to prepare a 1000 (mg L^{-1}) ppm Cr(VI) stock solution. Besides, hexavalent chromium concentrations of 0, 10, 20, and up to 100 mg L^{-1} were prepared and a calibration curve was plotted using these concentrations and the corresponding absorbance.[17]

2.5 Preliminary study on the effect of the adsorption parameters

Using the one variable-at-a-time approach, the effect of each parameter on the chromium adsorption uptake capacity of the activated carbon products was investigated. Specifically, adsorption times in the range of 30–210 min, pH values of 1–7, adsorbent load of 0.5 to 3.5 g L^{-1}, and initial chromium concentration of 20–80 mg L^{-1} were considered. Only the effect of one variable was investigated in this approach, while the others were kept constant. Hence, by changing the adsorption time from 30 to 210 min at 30 min intervals and fixing the pH at 3, adsorbent dose at 1.5 g L^{-1}, and chromium concentration at 40 mg L^{-1}, the effect of the time on the adsorption process of chromium with activated BP was studied.[28] Similarly, the effect of each adsorption process parameter under different conditions was investigated in their respective range (Table 2).

The adsorption process was performed in Erlenmeyer flasks, in which the adsorbate and adsorbent were allowed to contact at a fixed magnetic agitation of 300 rpm. After passing the filtrate through Whatman filter paper, the amount of residual chromium was measured. The removal efficiency of activated BP was determined using eqn (1). The concentration of hexavalent chromium (Cr(VI)) after the adsorption was determined using a UV-spectrophotometer and a calibration curve. Each experiment in the spectroscopy analyses was conducted by pouring the filtrate into a cuvette and adding diphenyl carbazide solution dropwise to specifically quantify the available hexavalent chromium in the solution.[28]

$$R(\%) = \frac{(C_0 - C_f)}{C_0} \times 100 \quad (1)$$

where R (%) is the removal efficiency and C_0 (mg L^{-1}) and C_t (mg L^{-1}) are the initial and final Cr(VI) concentrations, respectively.

2.6 Model evaluation using RSM-CCD to study interaction effects

Several experiments were carried out to determine the interaction effects of the operational parameters simultaneously. Consequently, the preliminary data screening was used to determine the appropriate range of parameters and develop the experimental design using RSM-CCD (Table 3). Subsequently, statistical evaluations were performed to determine the correctness of the model. Next, the system output was adjusted and optimized using the model to yield the best possible outcome given the available operational parameters, which was designed to highlight any potential relationships among the operating parameters.

The total number of experiments required for 'n' independent parameters is $2n + 2n + c$, where c denotes the center point in the experiment.[29] Therefore, a total of 30 experimental runs was conducted separately for the experimental response of chromium removal efficiency and to discover the optimum conditions with six center-point experiments. Each experiment was conducted twice and average results were utilized. A mathematical model was selected to correlate the removal efficiency with all the factors. A quadratic model created by the Design Expert software was used to analyze the response surface regression for the design response, as given in eqn (2).

$$Y = \beta + \alpha_1X_1 + \alpha_2X_2 + \alpha_3X_3 + \alpha_4X_4 + b_1X_1X_2 + b_2X_1X_3 + b_3X_1X_4 + b_4X_2X_3 + b_5X_2X_4 + b_6X_3X_4 + c_1X_12 + c_2X_22 + c_3X_32 + c_4X_42 + \xi \quad (2)$$

where Y is the predicted response variable, β is the intercept constant, α_1–α_4 are the main linear effect constants, b_1–b_4 are the linear–linear coefficients, c_1–c_4 are the main quadratic effect coefficients, ξ is the error and X_1–X_4 are independent variables.[30]

2.7 Parameter optimization and evaluation of model performance

Statistical tests were performed with analysis of variance (ANOVA) and correlation coefficient (R^2) to evaluate the model equation performance and significance. To achieve a high removal efficiency using the activated BP, parameters such as time, adsorbent dose, pH, and Cr(VI) concentration were optimized through numerical optimization. The criteria set to solve the optimization are shown in Table 4. The optimal conditions were validated and confirmed with triplicate experimental data, and then the error was determined.

2.8 Kinetics of adsorption and isotherm studies

To examine the rate of Cr(VI) adsorption on the activated BP and to mathematically model the adsorption process, the kinetics and isotherm models of well-known models were studied.

2.8.1 Adsorption kinetics. The dynamics of the adsorption process, also known as kinetics, defines how quickly the

Table 2 Level of parameters for preliminary study

Factor	Level of parameters						
Time (min)	30	60	90	120	150	180	210
pH	1	2	3	4	5	6	7
Adsorbent dose (g L^{-1})	0.5	1	1.5	2	2.5	3	3.5
Initial concentration (mg L^{-1})	20	30	40	50	60	70	80

Table 3 RSM-CCD experiment parameter levels

Factor	Factor code	Level of parameters	
		Lower	Upper
Adsorption time (min)	X_1	60	120
pH	X_2	2	4
Adsorbent dose (g L^{-1})	X_3	1	2
Initial conc. (mg L^{-1})	X_4	30	50

Table 4 Criteria for the optimization process of the parameters

Parameter	Criteria	Lower limit	Upper limit	Importance
Time	Minimum	60	120	3
pH	In a range	2	4	3
Adsorbent dose	Minimum	1	2	3
Initial concentration	In a range	30	50	3
Removal efficiency	Maximum	38	94	3

adsorbent adsorbs the molecules of hexavalent chromium.[31,32] In a 500 mL flask, 1.5 g L^{-1} of the sample was added to 250 mL of chromium solution with a pH of 3.0 and an initial concentration of 40 mg L^{-1} to study the adsorption of Cr(VI) on the activated BP. A magnetic stirrer was used to agitate the solution at room temperature at 300 rpm. At various contact times of 10–180 min with a step of 10 min, the adsorption process was investigated. The trace concentration of chromium in each adsorption filtrate was examined. Using spectroscopy at a wavelength of 540 nm, the amount of chromium that was still present after adsorption in the specified period was analyzed.[32–34] The quantity of chromium adsorbed with time (q_t) was determined using eqn (3).[35] The pseudo-first-order and pseudo-second-order kinetic model non-linear equations (eqn (4) and (5), respectively) were fitted to the hexavalent chromium kinetics on the surface of the acid-activated BP samples, and the best fit was chosen based on the higher value of R^2.[36,37]

$$q_t = \frac{(C_0 - C_t)}{m} \times V \quad (3)$$

$$q_t = q_e\,(1 - e^{-k_1 t}) \quad (4)$$

$$q_t = q_e\left(\frac{q_e k_2 t}{(1 + q_e k_2 t)}\right) \quad (5)$$

where q_t (mg g^{-1}) is the quantity of adsorbate at time t, C_0 (mg L^{-1}) denotes the initial concentration of chromium, C_t (mg L^{-1}) is the Cr(VI) concentration at time t, V (L) is the volume of solution containing Cr(VI), and m (g) represent the adsorbent mass.

k_1 and k_2 are the adsorption rate constant in min^{-1} and g mg^{-1} min^{-1}, respectively. The adsorbate at equilibrium (q_e) was calculated using eqn (6).[35]

$$q_e = \frac{(C_0 - C_e) \times V}{m} \quad (6)$$

where q_e (mg L^{-1}) denotes the equilibrium adsorption capacity.

According to the non-linear curve of t *versus* q_t, all the kinetic parameters (k_1, k_2 and q_e) were determined.

2.8.2 Adsorption isotherm models. The most reliable isotherm models for predicting equilibrium adsorption processes mathematically are the Langmuir and Freundlich models. The Langmuir model predicts the adsorption capability of the adsorbent when a monolayer is completely formed on its surface. Alternatively, according to the Freundlich model, adsorption takes place on different surfaces.[38] Thus, to determine the most suitable model, different experiments were conducted.

In the adsorption isotherm experiments, 500 mL of various initial Cr(VI) concentrations of 20, 40, 60, 80, 100, and 120 mg L^{-1} as the adsorbate were mixed with 1.5 g L^{-1} of adsorbent at a pH of 3.0. The adsorption process was carried out by stirring for 5 h using a magnetic stirrer. Following each adsorption, the adsorbent was filtered, the equilibrium concentrations were ascertained by UV spectroscopy, and the analogous amount of adsorbate at equilibrium (q_e) was computed. The non-linear equation for the Langmuir isotherm model is provided by eqn (7).

$$q_e = q_{max}\,(K_L C_e)/(1 + K_L C_e) \quad (7)$$

where K_L is the Langmuir equilibrium constant in L mg^{-1}, C_e is the equilibrium adsorbate concentration in mL L^{-1}, and q_{max} is the total equilibrium monolayer sorption capacity in mg g^{-1}. The Langmuir constants q_{max} and K_L were computed from the nonlinear regression of the experimental data as q_e *versus* C_e.

Furthermore, eqn (8) represents the non-linear Freundlich isotherm model to which the experimental data was fitted.

$$q_e = K_F C_e^{1/n} \quad (8)$$

where K_F represents the adsorption capacity Freundlich constant and n the adsorption intensity Freundlich constant. Similarly, K_F and n were determined from the nonlinear regression of the C_e *versus* q_e experimental data.[39]

2.9 Recyclability study

Desorption and adsorbent regeneration studies were performed in a beaker, where 1.5 g adsorbent was mixed with 100 mL solution and shaken for 2 h at 300 rpm. The precipitate was collected and rinsed with distilled water repeatedly until the filtrate pH was 7.0. Subsequently, the Cr(VI)-loaded adsorbent was soaked for 2 h in a 400 mL, 0.05 M NaOH solution. Then, the adsorbent was collected and used again for adsorption. The UV-vis spectra at 540 nm were recorded to examine the supernatant solutions.[40] The adsorption and desorption operations were repeated seven times in total.

3 Results and discussion

3.1 The removal efficiency of activated BP

BP was activated at different activation times in the range of 1–3 h, with activation temperatures in the range of 350 °C to 550 °C and phosphorus acid concentration in the range of 10% to 90%. The activation process was conducted by changing one

variable and keeping the other two parameters constant (Fig. 1(a)–(c)). The removal efficiency of the activated BP as a function of activation time of 1, 1.5, 2, 2.5, and 3 h at an activation temperature of 450 °C and 50% phosphoric acid is shown in Fig. 1(a). The results unequivocally demonstrate that when the activation time increased from 1 h to 2 h, the efficiency of the activated BP increased from 78% to 98.2%. After 2 h, the removal efficacy surged slightly, and then remained almost constant. This showed that the activation process improves the adsorption performance of the activated banana peel. This may be due to the removal of volatile components in BP as it was subjected to a prolonged activation time at 450 °C. Besides, it seems that the surface area of the activated BP increased as a result of the porosity created when the volatile components evaporated.[41]

The removal efficacy of the adsorbent with respect to activation temperature in the range of 350 °C to 550 °C at an activation time of 2 h and 50% acid concentration is described in Fig. 1(b). The effectiveness of the activated BP increased from 69% to 98.6% when the activation temperature varied from 350 °C to 450 °C and declined to 45% as the activation temperature further increased to 550 °C. This experiment revealed that the activation temperature has a positive and negative effect on the adsorption capacity of the activated BP. Activating BP at a temperature of 450 °C increased its surface area, and thus its removal ability. However, its performance declined at higher temperatures, as can be observed in Fig. 1(b). The lower removal efficiency of activated BP at higher temperatures can be attributed to the decomposition of the sample at activation temperatures higher than 450 °C.[42]

Fig. 1(c) depicts the removal efficacy of the activated BP as a function of phosphoric acid concentration. At a temperature of 450 °C and activation time of 2 h, the efficiency was determined in acid concentrations in the range of 10–90%. Fig. 1(c) shows that as the acid concentration changed from 10% to 50%, the removal efficiency of the activated BP increased from 66% to 97.6%. When the acid concentration increased to 90%, the performance of the activated BP dropped dramatically to 76.5%. The increased removal efficiency indicates that the acid reacts with the impurities and washes them out. However, due to the reactive nature of strong acid, BP lost its adsorption properties at higher acid concentrations, *i.e.*, above 60%.[43]

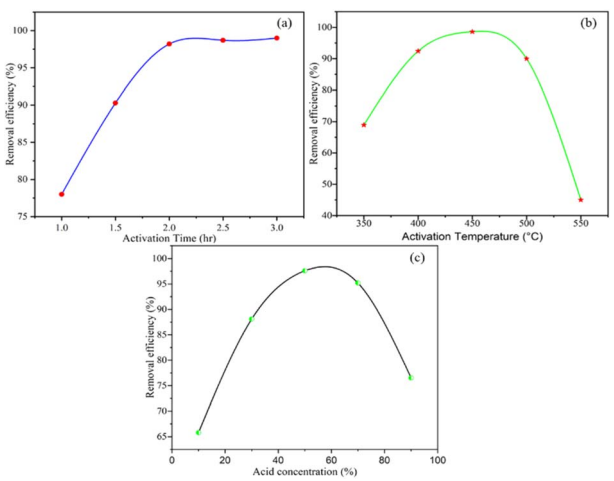

Fig. 1 Removal efficiency as a function of (a) activation time, (b) activation temperature, and (c) acid concentration.

Besides the interactive effect of each parameter of the activation process of BP, it can be deduced from these experiments that the best activated BP was produced at an activation time of 2 h, activation temperature of 450 °C, and acid concentration of 50%. Accordingly, BP specifically activated at 2 h, 450 °C, and 50% acid was characterized for further application.

3.2 Characteristics of adsorbent (activated BP) and raw BP

The raw and chemically and thermally activated BP were characterized using different techniques, namely, proximate analyses, SEM, BET, and FTIR.

3.2.1 Analysis of proximate results. Table 5 shows the moisture content, volatile material, fixed carbon content, and ash content results for the raw and activated BP using the ASTM standard methods. It can be seen that the moisture content of the well-activated BP is much less than the prepared raw BP. Previous studies by Kramarenko *et al.* and others showed that activated BP has a moisture content of about 5–7% and raw BP has a moisture content in the range of 7–10%. It can also be observed from the TGA analysis that the activated BP maintained a nearly constant weight up to 300 °C, indicating that a considerable amount of water was already removed.[44–46]

3.2.2 Elemental analysis. The CHNS/O analysis of the raw and activated BP is summarized in Table 6. The carbon content of the raw BP was found to be 44.54%, indicating its significant potential application as an adsorbent. The activation of BP substantially increased the carbon content to 64.67% and reduced the content of oxygen by 35% compared to raw BP. This may be due to the removal of some volatile components during the chemical treatment and the breakdown of the double-bonded carbon in the calcination process.[47] Also, N and S showed a very small change after the activation process.

3.2.3 FTIR analysis. Fig. 2 depicts the FTIR spectra of the raw and activated BP. The spectra revealed the presence of some functional groups in both samples with peaks located at wavenumbers of 3349.8, 2927.5, 1710.6, 1602.6, 1384.7, and 1035.6 cm^{-1}. The weak peak at 3349.8 cm^{-1} indicates the presence of moisture, most likely in the OH group. The incidence of stretching in the C–H alkane group may explain the peak at 2927.5 cm^{-1}. Furthermore, an aromatic compound, specifically the C–H stretching group, can be assumed to exist

Table 5 Proximate analysis results for raw and activated BP

	Result (%)	
Parameter	Raw	Activated
Moisture content	9.2 ± 0.02	6.1 ± 0.02
Volatile content	18 ± 0.01	15.93 ± 0.03
Ash content	5 ± 0.04	4.5 ± 0.05
Fixed carbon	67.8 ± 0.03	73.47 ± 0.04

Table 6 Elemental analysis of raw and activated BP[a]

	Elemental composition (%)	
Element	Raw BP	Activated BP
Carbon (C)	44.54	64.67
Hydrogen (H)	7.24	3.74
Nitrogen (N)	1.26	1.24
Sulfur (S)	0.053	0.048
Oxygen (O)[diff.]	46.91	30.302

[a] diff. = 100 − (C + H + N + S).

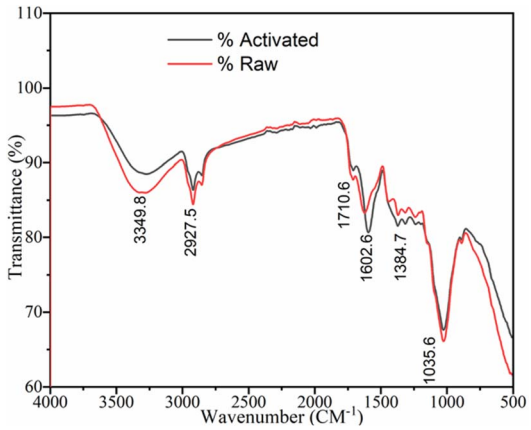

Fig. 2 FTIR-spectra of raw and activated BP.

due to the weak peak of 1710.6 cm^{-1}. The presence of the C=C stretching group, O–H bending phenol, and C–N amine group in the sample is indicated by the medium-intensity peaks located at 1602.6, 1384.7, and 1035.6 cm^{-1}, respectively. More precisely, the transition of one or more strong peak patterns to weak peak patterns may indicate that some or all the compounds, including water, were eliminated during the calcination process. The two spectra have a similar pattern but differ in the number of functional groups available. These results are also consistent with the recent studies by T. A. Aragaw and others, who recorded the spectra of raw and activated BP, matching with the spectra in the present study.[48–50]

3.2.4 BET analyses. The surface area and pore volume according to the nitrogen adsorption–desorption isotherms for the raw and activated BP (before and after adsorption) were studied and BET analyses were performed. The surface area of the raw and activated BP before and after adsorption was found to be 10 $m^2\ g^{-1}$, 200 $m^2\ g^{-1}$, and 80 $m^2\ g^{-1}$, respectively. This gives clear information that the activation process produced a relatively high surface area. Moreover, the BET result after adsorption revealed that most of the surface is occupied by adsorbate molecules. Fig. 3 displays the N_2 adsorption–desorption isotherms and the pore size distribution curves of the raw BP, activated BP, and activated BP after the absorption of Cr(VI). The isothermal curves of the raw, activated BP, and activated BP following Cr(VI) adsorption differed significantly,

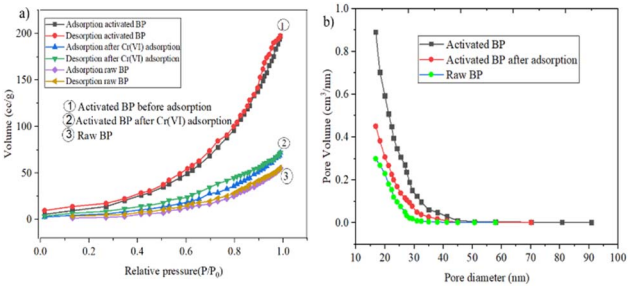

Fig. 3 Nitrogen adsorption–desorption isotherms curves (a) and pore size distribution of activated BP, raw BP, and after Cr(VI) absorption (b).

indicating differences in their adsorption behaviors. This suggests that BP activation modifies the pore structure and produces high porosity, which is consistent with the BET analysis reported by Rashudi *et al.*[51]

3.2.5 SEM analyses. The SEM results of both the activated BP before and after the adsorption process are demonstrated in Fig. 4(a) and (b), respectively. It was revealed that the activated BP before adsorption was more porous than the activated BP after hexavalent chromium was adsorbed on its surface. Moreover, the SEM image shows that most of the surface of the adsorbent is occupied by the adsorbate. A similar result in terms of porosity can be seen from the previous work, where the porosity was coated with the adsorbate.[52]

3.2.6 XRD analysis. The XRD pattern of the activated BP is shown in Fig. 5, showing the presence of broad and weak diffraction peaks located at 2θ values of 26° and 46°, respectively. This result suggests that activated BP contains graphite crystallite. The presence of graphite crystallites in the activated BP could have interesting implications for its properties, namely, adsorption capacity. The above-mentioned peaks correspond to the 002 and 100 planes of the carbon material, respectively.[22] The crystallite size of the activated BP based on these two peaks (46° and 26°) is 37.91 and 15.07 nm, respectively, with an average crystal size of 26.5 nm.

3.2.7 TGA analyses. The thermal decomposition of the raw and activated BP was studied to determine the effect of temperature and compare the raw material and the product under oxidized conditions. According to Fig. 6, the activated BP began to decompose after 500 °C, whereas the raw BP started to decompose after 350 °C. The release of bound water and other

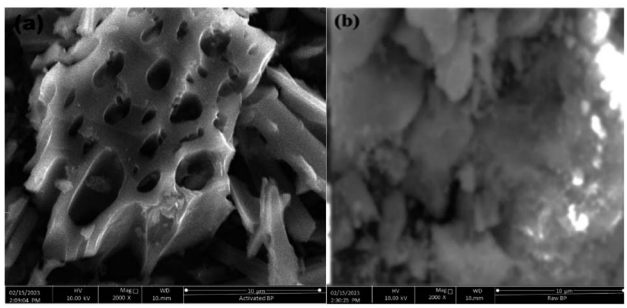

Fig. 4 Morphology study of activated BP (a) before and (b) after adsorption.

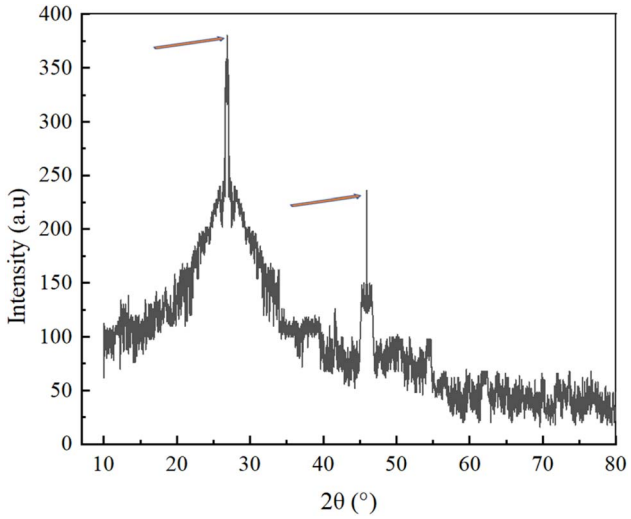

Fig. 5 XRD pattern of activated BP.

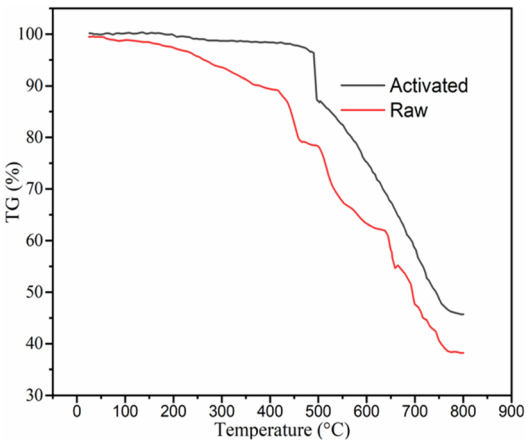

Fig. 6 TGA curves.

impurities may be responsible for the mass loss between 350 °C and 500 °C. The sample breaking down into smaller components, such as carbon dioxide, may be the cause of the steep decline in both curves above 600 °C.

3.2.8 Point of zero charge analysis. It can be observed from Fig. 7 that the point of zero charge of the activated BP is 5.83. The adsorbent surface chemical nature varied with the pH of the operating conditions. When the pH was less than the pH of point of zero charge, the adsorbent surface is considered positively charged, and when the adsorbent surface pH is above the pH of point of zero charge, the adsorbent is negatively charged. Thus, it can be deduced that the adsorbent surface is positively charged below a pH of 5.83 and negatively charged above a pH of 5.83. Moreover, the adsorption of Cr(VI) on activated BP seems more favorable below pH 5.83 conditions.

3.3 RSM-CCD experiment and parameter optimization

An initial investigation was carried out on the one variable-at-a-time method for the removal of Cr(VI) by adsorption utilizing the

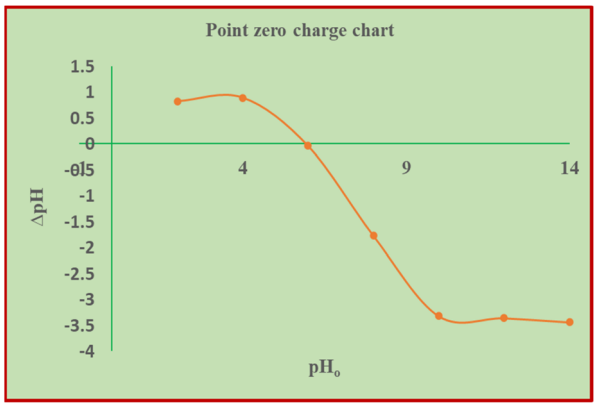

Fig. 7 Point of zero charge of activated banana peel.

activated BP and the interactive influence of process variables such as contact time, pH, adsorbent dosage, and initial concentration. Nature, especially regarding adsorption, does not work based on one set of parameters. Specifically, the parameters defining the process are interactive, with each variable influencing the others and the process as a whole. Thus, the effect of all the relevant parameters must be considered.

The chromium adsorption capacity of the activated BP as parameterized by the variables was determined by conducting the adsorption process on its surface. Subsequently, the trace amount of Cr(VI) remaining was quantified using UV-spectroscopy. The concentration was determined based on the standard calibration curve.

3.3.1 Individual parameter effect. The effect of individual parameters on the process adsorption was examined in the preliminary study by varying one parameter, while keeping the others constant (Fig. 8(a)–(d)).

3.3.1.1 Effect of contact time. The effect of contact time on the hexavalent chromium adsorption process on the surface of the activated BP at various times in the range of 30–210 min at 30 min intervals was studied at a fixed adsorbent dose of 1.5 g L^{-1}, pH of 3, and chromium initial concentration of 40 mg L^{-1}.

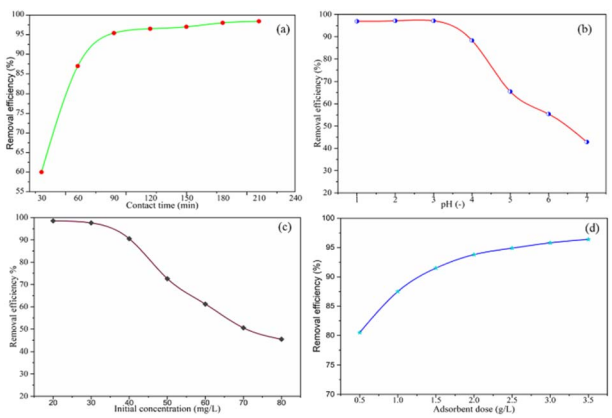

Fig. 8 Cr(VI) removal efficiency of activated BP with (a) contact time, (b) pH, (c) initial concentration and (d) adsorbent dose.

As depicted in Fig. 8(a), the chromium removal efficacy of the activated BP increased from 30% to 95% as the contact time increased from 20 to 60 min. However, as the adsorption duration was prolonged from 90 to 210 min, the removal efficiency increased slightly, and then tended to be constant. This may be the adsorption equilibrium point was approaching, and finally attained. This indicates that all, if not most of the surface available for hexavalent chromium is occupied. Moreover, the adsorption process is expected to slow down with time, and thus the driving force for adsorption decreases.[41]

3.3.1.2 Effect of pH. The effect of pH on the adsorption process of hexavalent chromium on the surface of the acid-activated BP at pH of 1.0, 2.0, 3.0, 4.0, 5.0, 6.0, 6.0, and 7.0 was studied at a fixed adsorbent dose of 1.5 g L^{-1}, contact time of 90 min, and initial chromium concentration of 40 mg L^{-1}. Fig. 8(b) shows that the activated BP has the highest chromium removal efficiency at around pH 1 and 3, which is approximately 98%. As the pH increased to 7, the removal efficiency decreased to 44%. Thereafter, the removal efficiency remained almost constant. The dependence of adsorption on pH is largely determined by the type and ionic state of the surface functional groups in the adsorbent and the metal chemistry in the solution.[53]

According to Afshin *et al.*,[28] at low pH, bichromate and dichromate become the predominant species in solution. Given that the point of zero charge of the solution is 5.83 pH, the charge of the adsorbent is positive at low pH and negative at higher pH. Therefore, OH^- ions seem to compete with the chromate ions when the pH increases, which causes the Cr(VI) adsorption capacity to decline sharply. Similarly, Gue *et al.* and other researchers discussed that Cr(VI) adsorption is more favorable at low pH values, preferably not more than pH 3.[29,54–56] When the pH exceeds 5.83, the amount of hydroxyl ions in the solution increases and metal ions react and precipitate with the OH^- ions, making biosorption impossible.[57] Therefore, the optimum pH seems to be in the vicinity of pH 2 to 3, given that a recent article stated that Cr^{6+} adsorption is more effective in acidic solution.[58]

3.3.1.3 Effect of initial concentration. At a fixed time of 90 min, pH of 3, and adsorbent dose of 1.5 g L^{-1}, the impact of the initial concentration of hexavalent chromium on the process of adsorption on the surface of the activated BP at 20, 30, 40, 50, 60, 70, and 80 mg L^{-1} was investigated. The chromium removal *versus* chromium initial concentration is shown in Fig. 8(c). As observed, when the initial concentration increased from 20 to 80 mg L^{-1}, the chromium removal efficiency rapidly decreased from 98.2% to 45%. The apparent reason for this decrease in efficiency with concentration is the disproportionate amount of adsorbent available for the adsorption of chromium. The graph shows that 1.5 g L^{-1} adsorbent is capable of adsorbing about 90% of chromium molecules when the concentration is below 40 mg L^{-1}. In this case, given that the amount of adsorbent remained constant at 1.5 g L^{-1}, it is inevitable that the removal efficiency sharply decreased with an increase in the concentration of chromium beyond 45 mg L^{-1}. This indicates that 1.5 g L^{-1} adsorbent at the given adsorption time and pH exceeds its adsorbing capacity limit at higher initial concentrations of chromium.

3.3.1.4 Effect of adsorbent dose. The impact of the dosage of the adsorbent on the adsorption process of hexavalent chromium using the activated BP at 0.5, 1.0, 1.5, 2.0, 2.5, 3.0, and 3.5 g L^{-1} was studied at a fixed contact time of 90 min, pH of 3 and chromium initial concentration of 40 mg L^{-1}. Fig. 8(d) shows the removal efficiency with the adsorbent dose. The removal efficiency of the activated BP increased from 80% to 94% as the adsorbent dose increased from 1 to 2 g L^{-1}. It is expected that the removal efficiency will increase with an increase in the adsorbent dose, where the amount of chromium adsorbed increases with the amount of adsorbent. This is because when the amount of adsorbent increases, there will be more space (surface) available for chromium molecules. Nevertheless, there are always limitations, including mass transfer and adsorption affinity, in this physical phenomenon to remove (adsorb) all the chromium in the solution. There was a decrease in the removal efficiency when the dosage was low. This may be owing to the small surface availability for adsorption. The adsorbent would adsorb proportional chromium and reach a point after which no further adsorption could occur. The excess chromium leftover certainly affects the efficiency. Thus, it can be inferred from the graph that it is uneconomical to use doses of 2.5 and 3 g L^{-1} given that the removal showed a change of less than 1%.

3.3.2 Optimization of parameters and their interaction effect. The effects of the individual parameters were used to determine the levels of the variables in the RSM-CCD study. In the adsorption process, the parameters were set as follows: contact time (60–120 min), adsorbent dose (1–2 g L^{-1}), pH (2–4), and initial concentration (30–50 mg L^{-1}). Around 30 runs were performed at various levels and the model, parameters, and terms that were used to optimize the process and validate the result were analyzed.

3.3.2.1 Model fitting and ANOVA. The Design Expert software builds a mathematical model that depicts the response as a function of the relevant variables using experimental data and non-linear regression. Next, process variables are optimized and 3D surface plots are produced using this model. The created mathematical model was statistically assessed considering the experimental data to determine whether it accurately captures the process in terms of the variables considered. The *P*-value and R^2 (coefficient determination) values describe how significant the model fit is. A significant and close relationship between the model-predicted response and the experimental data is indicated by a model with *P* values less than 0.05 and an R^2 near unity. Among the models proposed by the software, the quadratic model gave the best fit with a *P*-value of 0.0001 and R^2 value of 0.983. Eqn (9) presents the equation in quadratic form that predicts the hexavalent chromium removal efficiency of the activated BP as a function of initial chromium concentration, adsorbent dose, pH, and contact time.

$$\begin{aligned}\mathrm{RE}\ (\%) = {} & 25.1554 + 0.6339 \times A + 13.3566 \times B + 88.1102 \\ & \times C + 0.1560 \times D - 0.0016 \times AB - 0.0277 \\ & \times AC + 0.0150 \times AD + 2.6460 \times BC + 0.2230 \\ & \times BD + 0.0.3822 \times CD - 0.0048 \times A^2 - 5.3104 \\ & \times B^2 - 33.1485 \times C^2 - 0.0418 \times D^2 \end{aligned} \quad (9)$$

where RE is the removal efficiency in % and A, B, C, and D are the contact time, pH, adsorbent dose, and initial concentration, respectively.

The statistical significance of the main parameters and interaction terms was assessed using the P-values and F-values (Table 7). It can be seen from Table 7 that the independent variables are all significant and some of the interactive terms are also significant.

It is expected that the mathematical model-predicted response (removal efficiency) values and the actual values found from experimental data will be close. Both values were similar in this study because the R^2 is close to unity (0.983) and the P-value is less than 0.0001. The adjusted R^2 is 0.968 and the predicted R^2 is 0.905. The actual and predicted values along the four parameters are shown in Table 8. To further compare both the model-predicted and actual values, a graph of predicted values as a function of actual values was drawn, as depicted in Fig. 9. The R^2 of 0.983 of the graph indicates that the two values are reasonably close.

3.3.2.2 Interaction effect of variables. The relationship between pH and adsorption time and removal efficiency of the activated BP in the event of adsorbing hexavalent chromium solution is shown in Fig. 10(a)–(c). Fig. 10(a) shows the surface plot of removal efficiency *versus* pH and contact time. At an initial concentration of 40 mg L^{-1} and adsorbent dose of 1.5 g L^{-1}, it displays the interaction effect of pH and contact time. It was found that when the pH decreased from 4 to 3 and the contact time increased from 60 to 90 min, the removal efficiency increased from 69% to 93.5%. Above pH 3 and contact time of 90 min, the removal efficiency remained slightly constant. Thus, it can be inferred that the removal efficiency seems to have favorable operating conditions with pH of 3 and adsorption time of 90 min for a solution that contains 40 mg L^{-1} of hexavalent chromium and adsorbent dose of 1.5 g L^{-1}. The increase in removal efficiency as the adsorption process was extended for a prolonged time is apparent, which overcomes the mass transfer barrier and allows more adsorbate to be transferred from the high Cr(VI) concentration solution to the adsorbent.

In terms of a surface plot and contour plot, Fig. 10(b) shows the removal efficiency as a function of adsorption time and adsorbent dose. It reveals the interaction between the variables of adsorbent dose and contact time with the response (removal efficiency) at a pH of 3 and initial concentration of 40 mg L^{-1}. The plot indicates that the removal efficiency increased from 67% to 94% as the adsorbent dose increased from 1 g L^{-1} to 1.5 g L^{-1} and the contact time increased from 60 to 92 min. It is evident that an increase in the adsorbent dose and contact time caused the removal efficiency to increase. An increment in adsorbent dose implies more surface for adsorption, and hence higher removal efficiency. Besides, the longer the adsorption time, the higher the removal efficiency as the adsorbate gets sufficient time to be adsorbed. Thus, more room and time imply an enhanced efficiency. However, it tended to remain constant when equilibrium was attained and when the hexavalent chromium molecules were uptaken exhaustively.

The impact of contact time and initial concentration on the chromium(VI) removal efficiency at a fixed adsorbent dose of 1.5 g L^{-1} and pH of 3 is shown in Fig. 10(c). With a decrease in the initial hexavalent chromium concentration from 60 mg L^{-1} to 38 mg L^{-1} and an increase in the contact time from 60 to 95 min, the removal efficiency increased from 65% to 97%, as illustrated in Fig. 10(c). However, a reduction in the initial concentration and longer contact times had little effect on the removal efficiency. The decrease in removal efficiency with an increase in initial concentration can be attributed to two apparent reasons. At an adsorbent dose of 1.5 g L^{-1}, a higher concentration demands more surface for adsorption. In the case of a fixed available surface area, the efficiency tends to decline given that some molecules remain unabsorbed. Alternatively, the mass transfer restriction of the adsorption process becomes appreciable when most of the surface available is occupied. Also, the contact time has a remarkable effect on the adsorption efficiency

Table 7 Analysis of variance in terms of coded factors

Source	Sum of squares	df	Squares mean	F value	P-value prob > F	
Model	7549.15	14	539.22	63.62	<0.0001	Significant
A	2176.20	1	2176.20	256.78	<0.0001	
B	797.83	1	797.83	94.14	<0.0001	
C	529.22	1	529.22	62.44	<0.0001	
D	853.00	1	853.00	100.65	<0.0001	
AB	0.0384	1	0.0384	0.0045	0.9472	
AC	2.78	1	2.78	0.3275	0.5756	
AD	325.15	1	325.15	38.37	<0.0001	
BC	28.01	1	28.01	3.30	0.0891	
BD	79.53	1	79.53	9.38	0.0079	
CD	58.43	1	58.43	6.89	0.0191	
A^2	520.18	1	520.18	61.38	<0.0001	
B^2	773.49	1	773.49	91.27	<0.0001	
C^2	1883.70	1	1883.70	222.26	<0.0001	
D^2	480.02	1	480.02	56.64	<0.0001	
Residual	127.13	15	8.48			
Lack of fit	126.86	10	12.69	241.64	0.05141	Not significant

Table 8 Experimental design matrix used in RSM-CCD

Run	A: time (min)	B: pH	C: adsorbent dose (g L^{-1})	D: initial concentration (mg L^{-1})	Removal efficiency (%)	
					Actual	Predicted
1	60	4	1	30	57.43	59.70
2	120	4	1	50	69.09	68.20
3	60	2	1	30	81.54	78.24
4	60	2	2	50	59.19	60.42
5	30	3	1.5	40	59.29	56.90
6	120	2	1	50	78.60	78.01
7	60	4	2	50	54.39	56.09
8	90	3	1.5	40	93.10	93.36
9	60	2	1	50	47.33	49.02
10	90	3	1.5	60	66.64	64.70
11	90	3	1.5	40	93.59	93.36
12	90	3	1.5	40	93.30	93.36
13	120	2	2	50	85.75	87.75
14	60	4	1	50	39.69	39.40
15	90	3	0.5	40	48.80	50.82
16	120	4	2	30	75.26	77.85
17	120	2	2	30	93.59	91.29
18	90	5	1.5	40	59.88	60.59
19	60	4	2	30	70.76	68.75
20	90	3	1.5	40	93.30	93.36
21	150	3	1.5	40	94.28	94.99
22	90	3	1.5	40	93.20	93.36
23	120	4	1	30	74.28	70.47
24	120	2	1	30	86.63	89.20
25	90	1	1.5	40	86.04	83.65
26	90	3	1.5	20	88.30	88.55
27	90	3	1.5	40	93.69	93.36
28	90	3	2.5	40	73.30	69.60
29	120	4	2	50	82.52	83.22
30	60	2	2	30	76.83	82.00

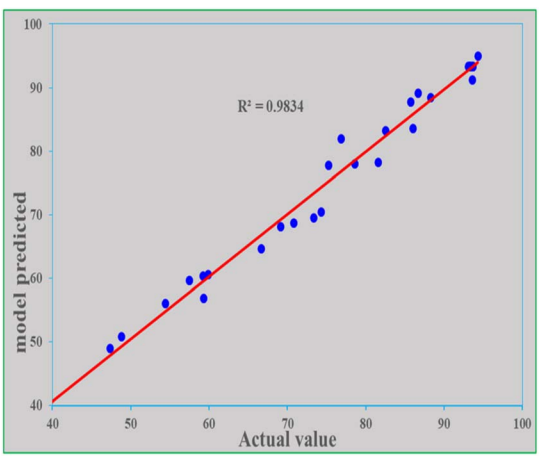

Fig. 9 Model-predicted *versus* experimental values.

as a step-wise process. On average, industrial wastewater contains no more than 30 mg L^{-1} Cr(VI).[59] Therefore, this will be the threshold limit in terms of initial concentration.

The interaction effect between pH and the adsorbent dose is depicted in Fig. 11(a) for a 3D surface with an initial concentration of 40 mg L^{-1} and an adsorption time of 90 min. As can be seen, the highest removal efficiency was found at around pH 2 and towards a higher adsorbent dosing. Thus, considering the effects of the parameters considered, the removal efficiency varied from 88.3% to 95%. It seems that pH 2 is the key operating condition to enhance the adsorption procedure.

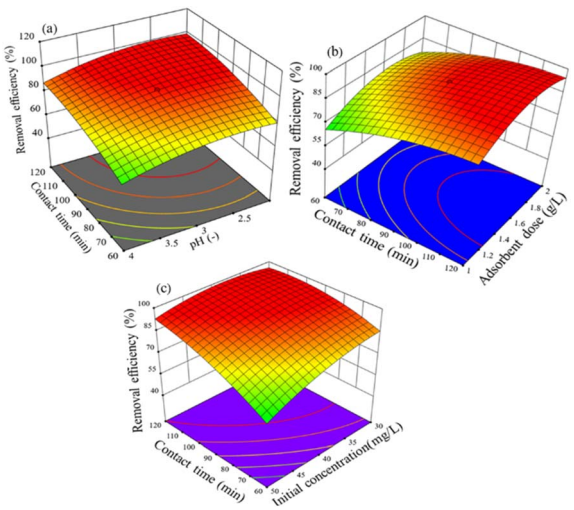

Fig. 10 Effect of parameters on Cr(VI) removal: (a) contact time and pH, (b) adsorbent dose and contact time, and (c) contact time and initial concentration.

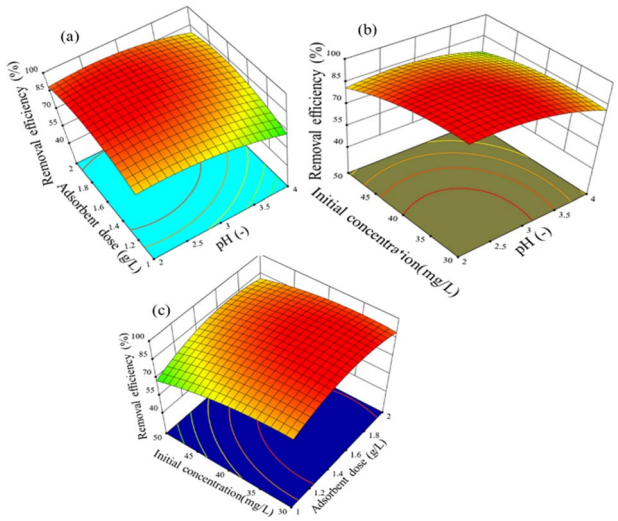

Fig. 11 Effect of parameters on Cr(VI) removal efficiency: (a) adsorbent dose and pH, (b) pH and initial concentration, and (c) adsorbent dose and initial concentration.

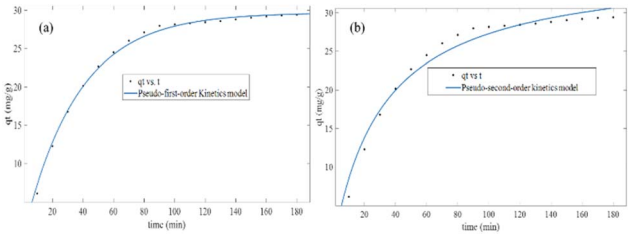

Fig. 12 Adsorption kinetics study using (a) pseudo first-order and (b) pseudo-second-order kinetics of Cr(VI) adsorption on activated BP surface.

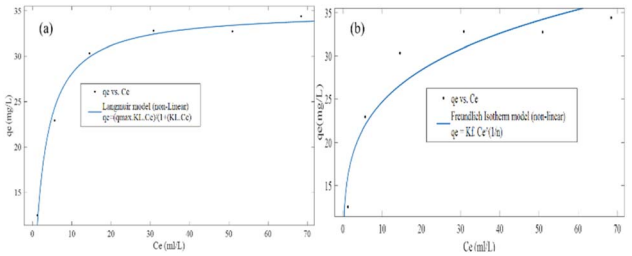

Fig. 13 Adsorption mechanisms on activated BP using Langmuir model (a) and Freundlich model (b).

The removal efficiency of hexavalent chromium by adsorption on the activated BP surface from aqueous chromium solutions is indicated in Fig. 11(b), which is displayed as a function of pH and initial concentration for 90 min with an adsorbent dose of 1.5 g L^{-1}. When the pH and initial concentration decreased from 4 to 2.5 and 50 mg L^{-1} to 36 mg L^{-1}, respectively, the removal efficiency increased from 75% to 97%. Fig. 11(b) presents evidence that the operating parameters for the maximum hexavalent chromium adsorption are low pH and low initial concentration. Generally, the wastewater from industries has low pH and chromium concentration (30 mg L^{-1}). Thus, the need for pre-treatment or pH adjustment can be avoided.[54]

Fig. 11(c) depicts the interaction effect of adsorbent dose and initial concentration on the removal efficiency at 90 min adsorption time and pH 3. As presented in Fig. 11(c), the removal efficiency increased from 69% to 95% when the adsorbent dose decreased from 2 g L^{-1} to 1.5 g L^{-1} and the initial concentration decreased from 50 mg L^{-1} to 36 mg L^{-1}.

3.3.2.3 Parameter optimization. The removal efficacy decreased with respect to initial concentration, with the adsorbent dose and time it increased, and at pH 3, the maximum efficiency was observed, while above pH 3 it tended to decrease sharply. Due to the trade-off among the parameters, this pattern requires optimization, which results in two-way effects. The variables were set in the study range to optimize the adsorption process, and the optimum value was adsorption time of 92 min, adsorbent dose of 1.5 g L^{-1}, pH of 3, and initial concentration of 38 mg L^{-1}. The best predictions of the model were verified by triplicate experiments conducted under the optimal conditions determined by numerical optimization (Table 9). The difference between the actual and predicted values was 0.05%. Consequently, it can be concluded that the fitted model significantly and reliably predicts the response.

3.4 Isotherm models and adsorption kinetics

3.4.1 Kinetics study. To understand the kinetics of hexavalent chromium adsorption on the activated BP, the pseudo-first-order and pseudo-second-order kinetics were examined, as presented in Fig. 12(a) and (b), respectively. The pseudo-first-order data from q_t *versus* t of adsorption were regressed using MATLAB nonlinear regression (Fig. 12(a)). Similarly, the pseudo-second-order kinetic equation was analyzed and the experimental results presented in Fig. 12(b). The coefficients of determination were found to be 0.996 for the pseudo-first-order kinetics and 0.973 for the pseudo-second-order kinetics. Thus, it can be concluded that the hexavalent chromium adsorption process taking place on the surface of the activated BP is mathematically described by the pseudo-first-order kinetic

Table 9 Experimental response and model predicted under the optimal conditions

	Contact time (min)	Adsorbent dose (g L^{-1})	pH	Initial concentration (mg L^{-1})	Removal efficiency (%)
Predicted	92	1.5	3	38	94.6
Actual	92	1.5	3	38	95.1

Table 10 Summary of nonlinear kinetics and adsorption isotherm model parameters

Kinetic model	q_e (mg g^{-1})	K_1 (min^{-1})	K_2 (g (mg)$^{-1}$ min^{-1})		R^2
Pseudo-first-order	29.67	0.00285			0.996
Pseudo-second-order	36.09	—	0.00085		0.973
Isotherm models	q_m (mg g^{-1})	K_L (L mg^{-1})	K_F (mg g^{-1})	n	R^2
Langmuir	35.01	0.41			0.988
Freundlich	—	—	15.8	4.9	0.895

model. Besides, it is apparent that physical sorption existed between the homogeneous sorbent and the rate of sorption is directly related to the adsorbate concentration.[60]

3.4.2 Adsorption isotherm analysis. Before determining the final concentrations, equilibrium concentrations, and the amount of adsorbate at equilibrium, Cr(VI) concentrations of 20, 40, 60, 80, 100, and 120 mg L^{-1} were adsorbed on the surface of the activated BP.

In both the Langmuir and Freundlich isotherm models, the C_e *versus* q_e data were regressed using the MATLAB nonlinear regression method, as shown in Fig. 13(a) and (b) with the curve fitting coefficient of determination (R^2), respectively. The R^2 values were found to be 0.988 and 0.897 for the Langmuir and Freundlich isotherm models, respectively. Besides, the maximum sorption capacity at equilibrium was found to be 36.09 mg g^{-1} using the Langmuir isotherm model.

Based on the R^2 values determined using the Langmuir isotherm model and Freundlich isotherm model curve fittings, it seems that the behavior of hexavalent chromium adsorption on the activated BP surface is described best by the Langmuir isotherm model. Thus, it can be stated that the Cr(VI) adsorption on the activated carbon follows a monolayer pattern, and subsequently multilayer adsorption.[60] The adsorption capacity of the adsorbent was more than 35 mg g^{-1}, where 1 g of adsorbent could adsorb more than 35 mg of adsorbate. This is comparable to the adsorption capacity of 31.3 mg g^{-1} of activated carbon synthesized from coconut shell.[61] A summary of the results of the adsorption kinetics and isotherm models is presented in Table 10.

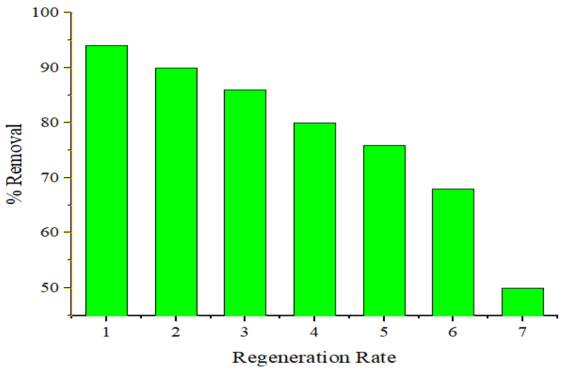

Fig. 14 Regeneration performance of activated BP.

3.5 Reusability of the adsorbent

As shown in Fig. 14, the removal efficiency decreased from 94% to 58% from run one to run seven due to the presence of a reduced amount of adsorbent compared with the initial removal efficiency for Cr(VI). The results display that the BP adsorbent presented a good cyclic adsorption performance with easy separation characteristics after adsorption due to its excellent regeneration properties, which can better meet the treatment requirements for industrial wastewater.

4. Conclusion

A promising activated carbon material was prepared from waste BP and shown to have potential as an adsorbent for the removal of Cr(VI) from tannery wastewater containing chromium and other heavy metals. The characterization methods revealed that the produced activated BP is a good adsorbent with considerable surface area, as determined by the BET analysis, and high porosity, as seen in the SEM images. The batch adsorption experiments revealed that the adsorbent was capable of removing most of the Cr(VI) from aqueous solution under the optimum operating conditions. It seems that the rate of adsorption of Cr(VI) on the adsorbent surface can mathematically be best modelled by the pseudo-first-order kinetic model and the behavior of adsorption follows the Langmuir isotherm model. Besides the experimental results for a synthetic aqueous solution of Cr(VI), the real wastewater study showed that the adsorbent has good potential for the removal of hexavalent chromium from effluents to the extent that it fulfils the standards. All the results showed that the adsorbent made from waste BP to remove Cr(VI), which is an efficient and cheap material, can be used repeatedly and keep the concentration of chromium in wastewater effluents within permissible limits.

Data availability

Most of data used in this study are presented in the article and if further data are required, it can be provided upon request.

Author contributions

Bereket Ameha – conceptualization, methodology, writing draft formal analysis, investigation, Tsegaye Sissay – resources, and

data curation, software, validation; Belay Getye – writing – review and editing; Shiferaw Ayalneh – revision and supervision, Talbachew Tadesse Nadew – visualization, and supervision; Destaw Agumass – manuscript revising and editing. After reading the manuscript, all authors have given their approval to publish it.

Conflicts of interest

The authors declare that there are no conflicts of interest regarding this article.

Acknowledgements

The authors would like to thank the Department of Chemical and Food Engineering, Faculty of Food and Chemical Engineering, Wollo University, Kombolcha, Ethiopia, Bahir Dar University, Bahir Dar, Ethiopia, and Addis Ababa Science Technology University, Addis Ababa, Ethiopia for their assistance in the research laboratory work.

References

1 F. M. Henretig, M. A. Kirk and C. A. McKay, Hazardous Chemical Emergencies and Poisonings, *N. Engl. J. Med.*, 2019, **380**, 1638–1655.
2 T. Wee, C. Kim and M. Hanif, Review on Wastewater Treatment Technologies, *Int. J. Appl. Environ. Sci.*, 2016, **11**, 111–126.
3 R. P. Singh and P. Singh, *Advances in Biological Treatment of Industrial Waste Water and Their Recycling for a Sustainable Future*, Springer Singapore, 2019, DOI: **10.1007/978-981-13-1468-1**.
4 M. Mokarram, A. Saber and V. Sheykhi, Effects of heavy metal contamination on river water quality due to release of industrial effluents, *J. Clean. Prod.*, 2020, **277**, 123380.
5 S. Renu, M. Agarwal and K. Singh, Heavy metal removal from wastewater using various adsorbents: a review, *J. Water Reuse Desalin.*, 2017, **7**, 387–419.
6 S. Mehdipour, V. Vatanpour and H.-R. Kariminia, Influence of ion interaction on lead removal by a polyamide nanofiltration membrane, *Desalination*, 2015, **362**, 84–92.
7 C. Zamora-Ledezma, *et al.*, Heavy metal water pollution: a fresh look about hazards, novel and conventional remediation methods, *Environ. Technol. Innov.*, 2021, **22**, 101504.
8 A. Singh, *et al.*, Heavy metal contamination of water and their toxic effect on living organisms, in *The Toxicity of Environmental Pollutants*, IntechOpen, 2022, vol. 34, pp. 57–67.
9 E. Kassahun, *et al.*, The Application of the Activated Carbon from Cordia africana Leaves for Adsorption of Chromium (III) from an Aqueous Solution, *J. Chem.*, 2022, **2022**, 1–11.
10 T. T. Nadew, M. Keana, T. Sisay, B. Getye and N. G. Habtu, Synthesis of activated carbon from banana peels for dye removal of an aqueous solution in textile industries: optimization, kinetics, and isotherm aspects, *Water Pract. Technol.*, 2023, **18**, 947–966.
11 M. L. Brusseau and J. F. Artiola, Chemical contaminants, in *Environmental and Pollution Science*, Elsevier, 2019, pp. 175–190, DOI: **10.1016/B978-0-12-814719-1.00012-4**.
12 M. Owlad, M. K. Aroua, W. A. W. Daud and S. Baroutian, Removal of hexavalent chromium-contaminated water and wastewater: a review, *Water. Air. Soil Pollut.*, 2009, **200**, 59–77.
13 D. Mohan, K. Singh and V. Singh, Trivalent chromium removal from wastewater using low cost activated carbon derived from agricultural waste material and activated carbon fabric cloth, *J. Hazard. Mater.*, 2016, **135**, 280–295.
14 S. Jha, R. Gaur, S. Shahabuddin and I. Tyagi, Biochar as Sustainable Alternative and Green Adsorbent for the Remediation of Noxious Pollutants: A Comprehensive Review, *Toxics*, 2023, **11**, 1–23.
15 S. Sharma and A. Bhattacharya, Drinking water contamination and treatment techniques, *Appl. Water Sci.*, 2017, **7**, 1043–1067.
16 V. S. Munagapati, *et al.*, Adsorptive removal of anionic dye (Reactive Black 5) from aqueous solution using chemically modified banana peel powder: kinetic, isotherm, thermodynamic, and reusability studies, *Int. J. Phytoremediation*, 2020, **22**, 267–278.
17 F. Pourramezani, F. Akrami Mohajeri, M. H. Salmani, A. Dehghani Tafti and E. Khalili Sadrabad, Evaluation of heavy metal concentration in imported black tea in Iran and consumer risk assessments, *Food Sci. Nutr.*, 2019, **7**, 4021–4026.
18 U. I. Aletan and H. A. Kwazo, Analysis of the Proximate Composition, Anti-Nutrients and Mineral Content of *Maerua Crassifolia* Leaves, *Niger. J. Basic Appl. Sci.*, 2020, **27**, 89–96.
19 Y. Chen, X. Mu, E. Lester and T. Wu, High efficiency synthesis of HKUST-1 under mild conditions with high BET surface area and CO2 uptake capacity, *Prog. Nat. Sci. Mater. Int.*, 2018, **28**, 584–589.
20 A. Turki, A. El Oudiani, S. Msahli and F. Sakli, Infrared Spectra for Alfa Fibers Treated with Thymol, *J. Glycobiol.*, 2018, **7**, 1–8.
21 J. F. Nohl, *et al.*, Low-voltage SEM of air-sensitive powders: from sample preparation to micro/nano analysis with secondary electron hyperspectral imaging, *Micron*, 2022, **156**, 103234.
22 Z. Xie, W. Guan, F. Ji, Z. Song and Y. Zhao, Production of Biologically Activated Carbon from Orange Peel and Landfill Leachate Subsequent Treatment Technology, *J. Chem.*, 2014, **2014**, 1–9.
23 N. Saadatkhah, *et al.*, Experimental methods in chemical engineering: thermogravimetric analysis—TGA, *Can. J. Chem. Eng.*, 2020, **98**, 34–43.
24 V. Kumar, V. Rehani, S. Saruchi and B. S. Kaith, Screening and optimization through response surface methodology for synthesis of pH, temperature and salt-sensitive Aloe vera –acrylic acid-based biodegradable hydrogel: its

evaluation as dye adsorbent, *Polym. Eng. Sci.*, 2019, **59**, 2323–2334.

25 E. N. Bakatula, D. Richard, C. M. Neculita and G. J. Zagury, Determination of point of zero charge of natural organic materials, *Environ. Sci. Pollut. Res.*, 2018, **25**, 7823–7833.

26 M. O. Saeed, K. Azizli, M. H. Isa and M. J. K. Bashir, Application of CCD in RSM to obtain optimize treatment of POME using Fenton oxidation process, *J. Water Process Eng.*, 2015, **8**, e7–e16.

27 K. K. Onchoke and S. A. Sasu, Determination of Hexavalent Chromium (Cr(VI)) Concentrations via Ion Chromatography and UV-Vis Spectrophotometry in Samples Collected from Nacogdoches Wastewater Treatment Plant, East Texas (USA), *Adv. Environ. Chem.*, 2016, **2016**, 1–10.

28 S. Afshin, *et al.*, Application of Box–Behnken design for optimizing parameters of hexavalent chromium removal from aqueous solutions using Fe3O4 loaded on activated carbon prepared from alga: kinetics and equilibrium study, *J. Water Process Eng.*, 2021, **42**, 102113.

29 C. Guo, L. Ding, X. Jin, H. Zhang and D. Zhang, Application of response surface methodology to optimize chromium (VI) removal from aqueous solution by cassava sludge-based activated carbon, *J. Environ. Chem. Eng.*, 2021, **9**, 104785.

30 S. Behboudi-Jobbehdar, C. Soukoulis, L. Yonekura and I. Fisk, Optimization of Spray-Drying Process Conditions for the Production of Maximally Viable Microencapsulated L. acidophilus NCIMB 701748, *Dry. Technol.*, 2013, **31**, 1274–1283.

31 P. Kumar and M. S. Chauhan, Adsorption of chromium (VI) from the synthetic aqueous solution using chemically modified dried water hyacinth roots, *J. Environ. Chem. Eng.*, 2019, **7**, 103218.

32 A. H. Shobier, M. M. El-Sadaawy and G. F. El-Said, Removal of hexavalent chromium by ecofriendly raw marine green alga Ulva fasciata: kinetic, thermodynamic and isotherm studies, *Egypt. J. Aquat. Res.*, 2020, **46**, 325–331.

33 C. Bai, L. Wang and Z. Zhu, Adsorption of Cr(III) and Pb(II) by graphene oxide/alginate hydrogel membrane: characterization, adsorption kinetics, isotherm and thermodynamics studies, *Int. J. Biol. Macromol.*, 2020, **147**, 898–910.

34 R. Khosravi, *et al.*, Chromium adsorption from aqueous solution using novel green nanocomposite: adsorbent characterization, isotherm, kinetic and thermodynamic investigation, *J. Mol. Liq.*, 2018, **256**, 163–174.

35 Y. Zhang, *et al.*, Recycling spent lithium-ion battery as adsorbents to remove aqueous heavy metals: adsorption kinetics, isotherms, and regeneration assessment, *Resour. Conserv. Recycl.*, 2020, **156**, 104688.

36 I. C. Afolabi, S. I. Popoola and O. S. Bello, Modeling pseudo-second-order kinetics of orange peel-paracetamol adsorption process using artificial neural network, *Chemom. Intell. Lab. Syst.*, 2020, **203**, 104053.

37 S. Han, *et al.*, Co-monomer polymer anion exchange resin for removing Cr(VI) contaminants: adsorption kinetics, mechanism and performance, *Sci. Total Environ.*, 2020, **709**, 136002.

38 M. A. Al-Ghouti and D. A. Da'ana, Guidelines for the use and interpretation of adsorption isotherm models: a review, *J. Hazard. Mater.*, 2020, **393**, 122383.

39 Y. Zhang, *et al.*, Waste eggshell membrane-assisted synthesis of magnetic CuFe2O4 nanomaterials with multifunctional properties (adsorptive, catalytic, antibacterial) for water remediation, *Colloids Surfaces A Physicochem. Eng. Asp.*, 2021, **612**, 125874.

40 H. B. Yang, *et al.*, Atomically dispersed Ni(i) as the active site for electrochemical CO2 reduction, *Nat. Energy*, 2018, **3**, 140–147.

41 J. Yang, *et al.*, Effects of Activation Temperature and Densification on Adsorption Performance of MOF MIL-100(Cr), *J. Chem. Eng. Data*, 2019, **64**, 5814–5823.

42 P. Gong, *et al.*, Extraction methods, chemical characterizations and biological activities of mushroom polysaccharides: a mini-review, *Carbohydr. Res.*, 2020, **494**, 108037.

43 J. Zhu, *et al.*, Effect of acid activation of palygorskite on their toluene adsorption behaviors, *Appl. Clay Sci.*, 2018, **159**, 60–67.

44 V. V. Kramarenko, A. N. Nikitenkov, I. A. Matveenko, V. Y. Molokov and Y. S. Vasilenko, Determination of water content in clay and organic soil using microwave oven, *IOP Conf. Ser. Earth Environ. Sci.*, 2016, **43**, 012029.

45 A. Arefnia, E. Momeni, D. J. Armaghani, K. A. Kassim and K. Ahmad, Effect of tire derived aggregate on maximum Dry Density of Kaolin, *J. Teknol. (Sciences Eng.)*, 2013, **66**, 19–23.

46 I. Hammouda and D. Mihoubi, Thermodynamic and mechanical characterisation of kaolin clay, *Polish J. Chem. Technol.*, 2014, **16**, 28–35.

47 M. K. Rai, *et al.*, Removal of hexavalent chromium Cr (VI) using activated carbon prepared from mango kernel activated with H3PO4, *Resour. Technol.*, 2016, **2**, S63–S70.

48 H. E. Shuma, L. L. Mkayula and Y. M. M. Makame, Assessment of the Effect of Acid Activation of Kaolin from Malangali on Water Defluoridation, *Tanzania J. Sci.*, 2019, **45**, 279–296.

49 T. A. Aragaw and F. Kuraz, *Advances of Science and Technology*, Springer International Publishing, 2019, vol. 274.

50 T. A. Aragaw and F. T. Angerasa, Synthesis and characterization of Ethiopian kaolin for the removal of basic yellow (BY 28) dye from aqueous solution as a potential adsorbent, *Heliyon*, 2020, **6**, e04975.

51 N. A. Rashidi, S. Yusup, A. Borhan and L. H. Loong, Experimental and modelling studies of carbon dioxide adsorption by porous biomass derived activated carbon, *Clean Technol. Environ. Policy*, 2014, **16**, 1353–1361.

52 E. Mosaddegh, A. Hassankhani and H. Karimi-Maleh, Synthesis and characterization of ES/Cu(OH)2 nanocomposite: a novel and high effective catalyst in the green synthesis of pyrano[4,3-b]pyrans, *Mater. Sci. Eng. C*, 2015, **46**, 264–269.

53 C. Luo, Z. Tian, B. Yang, L. Zhang and S. Yan, Manganese dioxide/iron oxide/acid oxidized multi-walled carbon nanotube magnetic nanocomposite for enhanced hexavalent chromium removal, *Chem. Eng. J.*, 2013, **234**, 266–275.

54 A. A. Attia, S. A. Khedr and S. A. Elkholy, Adsorption of chromium ion (VI) by acid activated carbon, *Brazilian J. Chem. Eng.*, 2010, **27**, 183–193.

55 T. Ravi and S. Sundararaman, Synthesis and characterization of chicken eggshell powder coated magnetic nano adsorbent by an ultrasonic bath assisted co-precipitation for Cr(VI) removal from its aqueous mixture, *J. Environ. Chem. Eng.*, 2020, **8**, 103877.

56 D. Pathania, A. K. Srivastava and A. Sharma, Bio-inspired fabrication of Cu–ZrO2 nanocomposites for the remediation of Cr(VI) from water system, *Curr. Res. Green Sustain. Chem.*, 2021, **4**, 100073.

57 R. R. De. Chimie, Recent advances in biosorption of heavy metals: support tools for biosorption equilibrium, kinetics and mechanism, *Rom. Acad.*, 2014, **59**(6–7), 527–538.

58 Y. Xu, *et al.*, Adsorption and reduction of chromium(VI) from aqueous solution using polypyrrole/calcium rectorite composite adsorbent, *Water Res*, 2019, **160**, 148–157.

59 V. Dhiman and N. Kondal, ZnO Nanoadsorbents: a potent material for removal of heavy metal ions from wastewater, *Colloid Interface Sci. Commun.*, 2021, **41**, 100380.

60 A. Blanco-Flores, *et al.*, Efficient removal of crystal violet dye from aqueous solutions by vitreous tuff mineral, *Environ. Technol.*, 2014, **35**, 1508–1519.

61 M. D. Vedenyapina, A. Y. Kurmysheva, S. A. Kulaishin and Y. G. Kryazhev, Adsorption of Heavy Metals on Activated Carbons (A Review), *Solid Fuel Chem*, 2021, **55**, 83–104.